Chapter 2

Biological Image Background Correction

This chapter is based on the following publication:

F. Cai, and F.J. Verbeek. "Dam-based rolling ball with fuzzy-rough constraints, a new background subtraction algorithm for image analysis in microscopy." Image Processing Theory, Tools and Applications (IPTA), 2015 International Conference on. IEEE, 2015.

F. Cai, and F.J. Verbeek. "Dam-based rolling ball with fuzzy-rough constraints, a new background subtraction algorithm for image analysis in microscopy." Submitted.

Chapter summary

Light microscopy is one of the important techniques in bio-imaging data analysis. The measurements obtained from images provide information on the concentration of molecules in cells, tissues, as well as whole mount. Microscopy images as they are acquired are not ideal; images, specifically shapes and textures often suffer from an uneven background due to flaws in the illumination. The presence of inhomogeneous noise in images, which mostly attribute to factors related to the light path between camera and microscope, can significantly impact the accuracy of downstream measurements.

In this chapter, we seek to contribute to quantitative improvement on the quality of light microscope readouts based on the proposed Dam-Constrained Background Correction (DCBC) method. The strategy we present employs a combination of fuzzy logic and rough set theory to constrain a morphological path at the moment background correction process takes place. To illustrate the competence of this method, a state-of-the-art shading correction based on entropy minimization (EMI) and the frequently used morphological rolling ball method (RBA) are compared via applications on three typical datasets. The reported results and extensive numerical analysis indicate an applausive performance on the proposed method.

2.1. Introduction

The study of biological phenomena using light or fluorescent imaging has transformed optoelectronic signal from a qualitative localization test to quantitative tools for functional analysis. These give rise to, for instance, features such as distance, area, velocity and intensity. A digital image of a specimen is created by the detector in an optical system. Inevitably, errors occur in the process of image acquisition via the specimen, the microscope or the detector itself [1]. An important source of error is the inhomogeneity of the intensity in the background. Sometimes the fluorescence has a shorter exposure time which will result in capturing less emitted photons compared to a procedure of longer exposure time [2]. Collection of fewer photons means that the relative contribution of the noise increases. Additionally, background intensity will accumulate through the surrounding fluorescence/ light sources, which will confound experiment's goals. This result leads to an undesirable contribution of the background with respect to the signal of interests.

In order to apply quantitative measurements in microscopy, a notion of the background must be known and, if possible, it must be removed before measurements in the images. Henceforth, it is always desirable to correct the inhomogeneous background beforehand. Several techniques have become available to mitigate abovementioned problems, also known as intensity inhomogeneity, uneven background and shading (vignetting). The common approaches serve to reduce the amount of inhomogeneity in microscope images, are noticed as Background Correction Processing (BCP).

The work in this chapter introduces a novel retrospective approach, on the basis of mathematical morphology to achieve better performance in a more general way. The proposed method is unsupervised and mostly parameter free. It employs the concepts of fuzzy membership, and approximation of an assumption from the rough set theory which is used to constrain an objective function. Subsequently, inspired and improved by conventional RBA [5], a morphological "dam" is constructed to avoid introducing a topological distortion (artefact), and to eliminate the noisy background while producing an enhanced foreground.

The remainder of this chapter is organized as follows: Section 2.2 introduces research related to background correction methods. In Section 2.3, the notion of contextual knowledge is reviewed. In Section 2.4, description of the objective function and dam-building methodology is presented. Section 2.5 provides the experimental results of the evaluation, followed by discussion and conclusions in Section 2.6.

2.2. Related Work

Existing methods in microscopy for illumination-based background correction can be applied while acquiring images (priori) or after acquisition (posteriori). The main difference between these approaches is a priori correction employs additional images obtained at the time of image capturing; while in posteriori correction, the controlled images are not available and therefore an ideal (hypothetical) background model has to be assumed.

The methods of acquiring prior-knowledge usually employ the background (illumination) images. An additional image is often made by defocusing or removing the specimen from the field of view [3], just capturing the specimen in bright field or dark field mode [15]. Consecutive adjusting the settings of camera and microscope [16] is also of importance to help with resulting images. Yielding results by linear image calculator (transmittance as the ration of transmitted light through specimen), however, these methods cannot cope with objective shading, e.g. shading caused by variation in specimen thickness at transmission imaging or by a non-planar surface in reflecting imaging. More specifically, images acquired from standard or automated microscopes, even with white (dark) referencing, are generally adequate for visual inspection but not completely for quantitative image analysis [17]. Practically, when conditions are not carefully controlled, differences can be more substantial and introduced to downstream evaluations.

Various approaches, namely retrospective (posteriori) correction, have been reported to extract the characteristics of background from a single image that depend on nothing but the actual images acquired during experiments. These methods mostly manipulate the data in both time-domain and frequency-domain using different sorts of filters, e.g. low (high)-pass-filter, linear-filter, compensated Gaussian blurring, etc. [18]. The drawback of these methods, however, is the limitation of the object size and the comparative background scale. The background is assumed to be either darker or brighter than the foreground. Moreover, the overlap of objects with the background is kind of forbidden in restoration, otherwise the mixture of foreground signal will be eliminated while applying the corrections in the frequency domain. Meanwhile, a mathematical morphology structuring element based on the image landscape has been introduced [4] [21] [19], i.e. the rolling ball algorithm. With a pre-defined radius, a virtual ball rolls over the ground of the topographical pixel-landscape. Each pixel that contacts with the surface of the ball will be selected for further processing. These methods, however, have limitations in that they are imprecise in the estimation of a solution and portray uncertainty in the control of the path in the application of microscopy image sets. Another technique [2] [20] which assumes that the image background is more homogenous relative to foreground, and estimate a correction function over the background regions from original images.

Ideally, it is better to correct the images with a priori method as all retrospective approaches make assumptions over the image characteristics that are unlikely to be strictly satisfied in any arbitrary image. However, one should be aware that the reproducibility of acquiring sample images for priori correction requires laborious manipulation, while errors can be even introduced. In this manner, a way more efficient and feasible retrospective DCBC method is proposed in this chapter.

2.3. Primary Notation

A. Fuzzy theory bound

The notion of fuzzy set was firstly introduced in 1965, and pioneered by Zadeh [7], fuzzy logic-based system have been successfully utilized into various application areas. A fuzzy set is the class of objects that contains consecutive grades of membership, with which value ranged from zero to one. This index assigned a "fuzziness" characteristic to the set, meaning a level of belonging. Particularly, a conventional set, referred to as the crisp set (commonly used in k- and/or c-means) will have either a value of zero or one; i.e. a Boolean value. The fuzzy membership function can be written as:

$$\mu_A: U \rightarrow [0,1] \qquad \textbf{Equation 2-1}$$

Where *A* denotes the fuzzy set, and the mapping function μ_A, is the membership function of *A*, while *U* is the universe.

B. Rough theory bound

Proposed by Pawlak [8], rough set theory is an approach to assess imprecision and uncertainty. Objects in the universe characterized by the same information, or knowledge are indiscernible (similar) in the view of available information about them. The concept of the indiscernibility relation is the mathematical basis of rough set theory.

An information system is an aggregation $S= \langle U, A, V, f \rangle$, where *U* is a non-empty finite set of *N* objects $\{x_1, x_2, \dots, x_N\}$ called the universe, and *A* is also a non-empty set of attributes. *V* is a value set such that $a: U \rightarrow V_a$ for every $a \in V$. With every subset of attributes *B* from *A*, we have $B \subseteq A$. We define an equivalence relation on *U* as:

$$I(B) = \{(x, y) \in U \times U: f_a(x) = f_a(y), \forall\, a \in B\} \qquad \textbf{Equation 2-2}$$

Elements belonging to *U* that can satisfy this equation (relation) *I(B)* are objects with the same value for attributes *B* and therefore, these objects are indiscernible with

respect to *B*. Moreover, an equivalence class containing the element *x* will be defined as *I(B)(x)*, in short *B(x)*. The classes of the equivalence sets are the basic concept of *B*. Given any subset of attributes *B*, with concept of $X \in U$ can be approximately defined by employing two exact sets respectively referred to as the lower and the upper approximation sets:

$$BD_*(X) = \{x \in U : B(x) \subseteq X\}$$
$$BD^*(X) = \{x \in U : B(x) \cap X \neq \emptyset\} \qquad \textbf{Equation 2-3}$$

Assigning to every subset *X* of universe *U*, a subset $BD_*(X)$ is referred to as the B-lower approximation of *X*, which can be classified as elements of *X* in the concept of *B*. While $BD^*(X)$ is the upper approximation which elements most probably belong to *X* given the knowledge *B*. The exactness based on the approximation set can be expressed by:

$$\alpha_B(X) = \frac{|BD_*(X)|}{|BD^*(X)|}, \qquad \text{for } X \neq \emptyset \qquad \textbf{Equation 2-4}$$

This equation is referred to as the accuracy of the approximation, where |.| denotes the cardinality of the sets. The accuracy measure captures the degree of completeness of the knowledge about the set *X*. According to the extended report in [9], we obtain a measurement of the roughness index by rewriting the Equation 2-4 as:

$$\rho_r = 1 - \alpha_B(X) \qquad \textbf{Equation 2-5}$$

From this normalized definition it holds that for every *B* and $X \subseteq U$, if $\rho_r = 0$, then the boundary region set *X* is empty. From this moment on, *X* is notated as *B*-definable, e.g. *X* is a crisp set with respect to the knowledge *B*. Otherwise, if $\rho_r > 0$, then this means *X* is *B*-undefinable, e.g. *X* is rough or uncertain with respect to the knowledge *B*.

2.4. Dam-Constraint Background Correction Strategy

A. Classical rolling ball concept

The quantitative measurement of (pixel-) intensity is a mixture of signal and background noise. It can be well estimated by measuring the local background pixels in the region of interest [10]. This procedure can be written as:

$$F_{obj} = \sum_{m=1}^{m-N_{obj}} F_{obj} - N_{obj} \frac{\sum_{n=1}^{n=N_{bkg}} F_{bkg}}{N_{bkg}} \qquad \textbf{Equation 2-6}$$

Where *F* is the fluorescent signal measured at each pixel (*m*, *n*), *obj* is the object, *bkg* is the selected background area or volume, and *N* is the number of pixels in the

selected object or background. This equation describes the framework of the RBA approach by computing the contribution of the background noise per pixel. By taking both advantages, we aggregate the classical RBA algorithm with the concept of fuzzy logic and rough theory to the image domain.

B. Selection of crest and toe for dam

Tedious signals are introduced often attribute to over-processing. The main goal of constructing a "dam" in DCBC method is to constrain the path of the morphological ball rolling into either the valley or summit image landscape, which does not meet our anticipation (selection of proper background). In this manner, a dam with crest and toe are established. This can be formulated into a bimodal threshold modelling on the basis of the composition of objects in the microscope images (cf. Figure 2-1 for instance, which objects foreground are assumed to consist of foreground and sub-foreground). Under the constraint of a dam, original information of a local region of interest will be preserved as much as possible, while over-segmentation will be limited (cf. Figure 2-2).

For a local region of interest, we have to obtain the multi-threshold values in order to construct a dam with a certain crest and toe in the image-landscape. Let x_{mn} be the pixel value with respect to the region size $m \times n$, and will obtain two average grey levels.

$$t_0 = \frac{1}{i}\sum_m \sum_n x_{mn}\ , \quad x_{mn} < t$$

$$t_1 = \frac{1}{j}\sum_m \sum_n x_{mn}\ , \quad x_{mn} \geq t \qquad \textbf{Equation 2-7}$$

where, i and j denote the number of occurrences of x_{mn} according to the threshold intensity-level t, and $i + j = m \times n$. Given by an initial threshold value t, the two average intensity-levels, t_0 and t_1, can be considered as a local background. In this manner two sets X_{t_0}, X_{t_1} are obtained with element x. The relationships of the pixels are $x \in X$, while their corresponding region should be directly depended on the change of the pixel values and the change in the local background. With respect to the membership function, taking the condition of these properties into account, we observed that the smaller the difference of the element pixel and its corresponding local background value, the larger the output of the membership will be. Notice that, it is expected one element should either belongs to set X_{t_0} or X_{t_1}. Consequently, this will result in a membership output value in an interval of 0.5 to 1. It is clear that the membership value equals one only if the element belongs to a crisp set, while it should also be monotonous within the domain of definition. With these notions, we thus obtain a piecewise function $g(x)$ and its convex formulation μ_X:

$$g(x) = \begin{cases} \frac{x_{mn}-t_0}{I_{max}-I_{min}}, & x_{mn} < t \\ \frac{x_{mn}-t_1}{I_{max}-I_{min}}, & x_{mn} \geq t \end{cases}$$ **Equation 2-8**

$$\mu_X(x_{mn}) = \frac{1}{2}[(g(x)-1)^2 + 1]$$ **Equation 2-9**

The I_{max} and I_{min} represent the maximum and minimum image intensity value. For a given value *t*, the membership value μ_X is in the interval [0.5, 1]. Moreover, the membership function μ_X has a convex shape in a line plot; this introduces a slight change of slope near 0.5 with much vagueness near the fuzzy centre (value 0.5), and a dramatic change of slope near 1 with a fast rate of convergence near the crisp point (value 1).

By definition, the fuzzy set is known as an approach to access the quantitative analysis of membership between the elements and sets. To this regard, we can obtain a performance measure of the fuzzy set segmentation result. This provides a better image landscape than the uniformity evaluation method. This is because uniformity is an index of indicating a degree of variance in a segmented region and the mean values belonging to this region. However, a shape evaluation is summary of a generalized gradient value for every pixel by checking the relationship between the determined threshold value and the grey values of its neighbouring pixels. Consequently, the more appropriate the threshold is chosen, the better the representation of resulting image landscape will be accomplished.

We assume that for the proposed bimodal thresholding method, the results of the first segmentation will separate the background and foreground, thereby containing the objects of interest. Then in a second segmentation of foreground, boundary domains (sub-foreground) will be isolated from objects. This procedure, for a better understanding, could take place when referring to cell cytoplasm and cell nucleus in cell microscope images. For our applications, the most likely shape we therefore will obtain is one in which all foreground pixels should contain cytoplasm and nucleus (cf. Figure 2-1). Successful partition of the nucleus from the maximum shape is required to define the boundary between the cytoplasm and the nucleus. Henceforth an upper-approximation set can be made as the pixels belonging to cytoplasm, whereas the nucleus is the lower-approximation set.

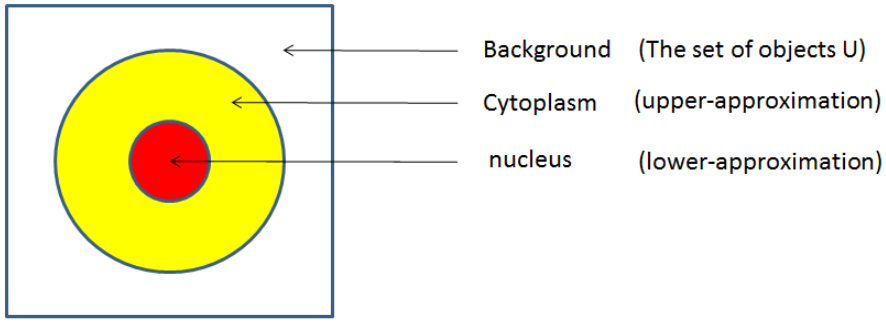

Figure 2-1. Illustration of rough-set reflection in a cell image. Boundary region is a subtraction of cytoplasm (yellow) by nucleus (red) region, while background (white) remains the same.

The upper-estimation of the rough set is estimated by assessing all neighbouring pixels for each pixel in the local region of interest:

$$P_{upper}(x,y) = \frac{2}{\sqrt{n}}\left(\sum_{i=1}^{n} |P_{n-neighboring} - P(x,y)|^2\right)^{\frac{1}{2}} \quad \textbf{Equation 2-10}$$

where n is the number of n-neighbouring pixels for each pixel. Practically, n=8 outperforms the other settings in our examination. The upper-approximation set is a collection of all points, which possibly belongs to one segmented region. In this manner, a correlation of spatial information with respect to those who have same or similar values is set up. The lower-approximation set contains original pixels that definitely belong to a class of known intensity, and therefore the roughness index ρ_r can be formulated as:

$$\rho_r = 1 - \alpha_B(X) = 1 - \frac{P(x,y)}{P_{upper}(x,y)} \quad \textbf{Equation 2-11}$$

The value of roughness index is large when the cardinality of the upper-approximation is larger than the original pixel value in the selected position. This typically occurs when there is large variance of the selected pixel with respect to its surrounding pixels; i.e. the intensity variation dramatically changes if there exists a boundary between two objects or regions. In other cases, the roughness index will be small, e.g. close to zero, as there is no significant change of intensity around a selected pixel.

After the two membership functions have been defined, they are combined by using a decision function, such as a parametric aggregation operator from the fuzzy set theory [11]. To simultaneously satisfy abovementioned criteria, while taken both

advantages from fuzzy logic and rough theory, it is of great importance to aggregate using the product t-Norm operation.

$$\mu_X(x) = A(x) = \rho_r(x) \oplus g(x)$$

$$\text{Subject to} \quad A(x) = \prod_{l=1}^{L} C_l(x) \qquad \textbf{Equation 2-12}$$

where $\oplus$ [1] is the aggregate operator and L=2. C_1 and C_2 correspond to $\rho_r(x)$ and $g(x)$ respectively. In this manner, a bi-objective function is aggregated into single-objective one for satisfaction. Note that, regarding to Equation 2-8, which consists of two partial equations that are depending on the local background, as well as on a temporary threshold *t*. It is essential that a correlation index allowing a membership function μ_X continuous weighting at local domain of definition. Therefore, we introduce a correlation function by taking the minimum and maximum intensity level into account, and weight each component of membership function μ_X as:

$$\wedge = \frac{1}{2} \cdot \frac{I_{max} - I_{min}}{I_{global\_max}} \qquad \textbf{Equation 2-13}$$

In Equation 2-13, I_{max} and I_{min} are the maximum and minimum value of local region respectively, while I_{global_max} is the maximum value in whole image. It is easily seen that the value of $\wedge$ will be in [0, 0.5]. Afterward, the bimodal thresholding cost function can be formulized as:

$$\mu_X(x_{mn}) = \rho_r(x) \oplus (\wedge \cdot g_{x_{mn}<t}(x) + (1-\wedge) \cdot g_{x_{mn}\geq t}(x)) \quad \textbf{Equation 2-14}$$

The appropriate measurement of uncertainty is the key to evaluate the degrees of vagueness whereas an element (pixel) belongs to a certain set (region) or not. Several approaches have been reported in recent decades, but in our case, we propose an evaluation based on Shannon's function to solve abovementioned uncertainty problems. From the information entropy theory [12], the measured entropy of the vagueness can also be experienced within a slightly changed definition:

$$E(X) = \frac{1}{MNln2} \sum_m \sum_n S(\mu_X(x_{mn})) \qquad \textbf{Equation 2-15}$$

Where *M* and *N* represent the size of the selected local region. Note that the given Equation 2-15 is monotonically decreasing in the interval [0.5, 1], but monotonically increasing in the interval [0, 0.5]. Hence, it is possible to minimize the lowest energy of the region rolled by the RBA ball path through Equation 2-15, while the definition zone is set to the interval [0.5, 1].

[1] To avoid confusion of the $\oplus$ symbol used in morphological processing as dilation operator.

C. Dam construction strategy

Background illumination correction based on mathematical morphology approach aims to find an estimation of illumination imperfections. For a "ball" rolling under the image landscape, it holds that those pixels the ball cannot touch will be kept in a smoothed foreground; e.g. the local minima and the peak. The smaller the radius of the ball, the deeper the topographical shape can be touched, and vice versa (cf. Figure 2-2). With the existing rolling ball (RBA) method there are some problems that effectuate uncertainty and imprecision in the resulting image. This morphological selection, attributing to over segmentation, will result in a loss of energy and details in the original image. To that end, the proposed method intends to produce a much smoother image and eliminate the artefacts by employing local threshold values t_0 and t_1 conducted from the results of minimization of local entropy, i.e. indicating the crest (t_0) and toe (t_1) of the dam.

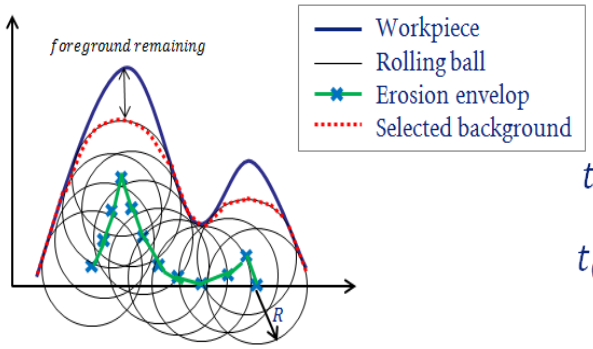

(a) Conventional Morphological BCP

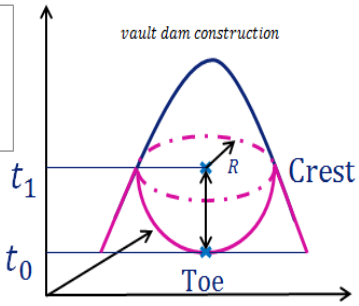

(b) Inllustration of constructing dam in 3D landscape

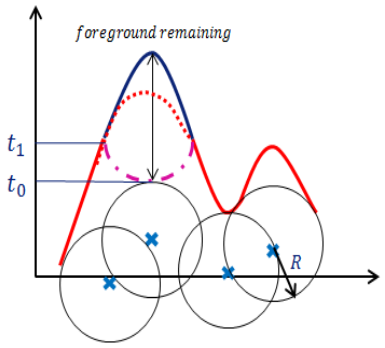

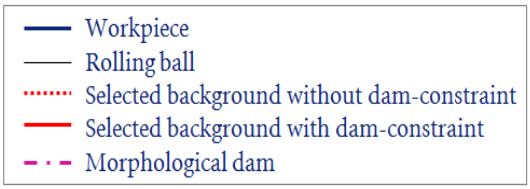

(c) Dam – constrained BCP

Figure 2-2. Process of constructing morphological dam in a 2D/3D image landscape. The ball path, with a predefine radius *R* (usually set in a range from 50 to 500 pixel), in either red line or dotted line depicts a solution of background selection. (a) classical rolling procedure of RBA in selecting background signal; (b) In a local region of interest, a vault dam is built with regard to local bi-thresholding values. The surface of dam is constructed on the basis of inversed equation (6). However, the extreme values are controlled by both t_0 and t_1; (c) illustration of background selection by means of approaches with and without dam-constraint, respectively.

Intuitively, the morphological ball in the proposed DCBC method, will not roll into the convex area, in which this region of interest is recognized as foreground. In other words, a suppression will occur if the ball is forced to rolling into the region with grey level between t_0 and t_1; and completely forbidden in the area with grey value higher than t_1 (cf. Figure 2-2). Be aware that, the smoothing factor of the foreground during morphological subtraction is relative to the radius of the rolling ball. Unlike the existing algorithm, which requires to be tuned for every step before adapting the ball to the object of interest, the proposed method is more robust as it includes an adaptive radius. The local region of interest is chosen as a sliding window with half the size of the original image, i.e. length and height is *m/2* and *n/2* respectively. Therefore, the radius of the ball is practically in an adaptive way, set as the *minimum (m/2, n/2)*. The procedure of proposed DCBC protocol is illustrated as in Figure 2-3.

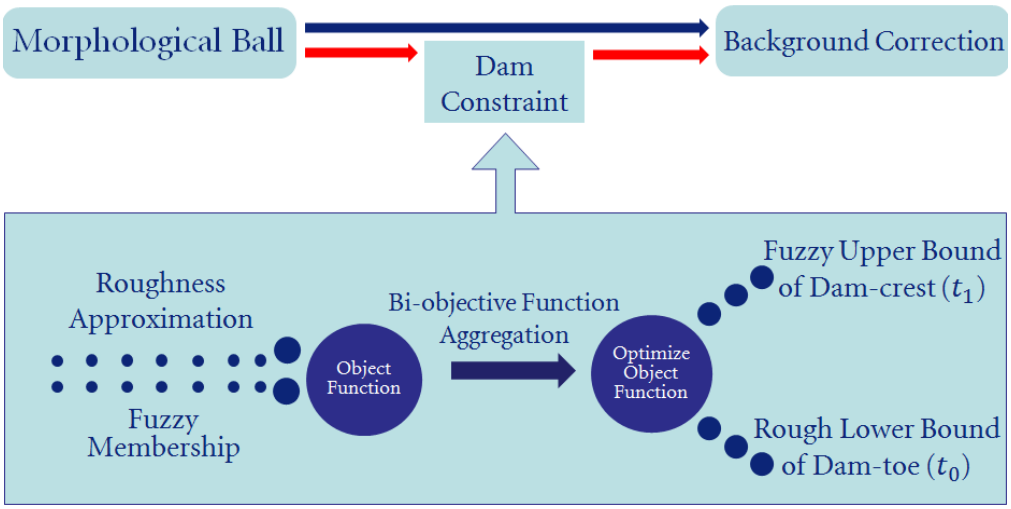

Figure 2-3. Workflow of proposed DCBC approach.

2.5. Experimental Results

A. Data acquisition

In order to assess the performance of proposed DCBC approach compared with state-of-the-art EMI and typical RBA method, characteristic images are employed. Image Set 1 is typical bright-field imaging, depicting cartilage cell cultures with bright background (256 x 256 pixels, 16 bit); these images were acquired with the standard Zeiss Bright Filed microscope. The other sets (set 2 and set 3) are typical multi-channel fluorescence sets depicting cultured cardiomyocytes with dark background (1024 x 1024 pixels, 8 bit; and 4704 x 3584 pixels, 8 bit); these sets are acquired with the BD-Pathway Imager [6]. Each dataset contains 12 samples in different growth stages. The evaluation methods are then implemented in qualitative and quantitative terms.

B. Qualitative tests

1) Artefact removal:

Information utilized for the further processing is actually kept in the background and artefacts are enhanced as well. Artefacts from the connection will, in general, occur between the edge or the corner of an image due to the start centre of conventional RBA and results in an embedded effect of the rolling ball. This is shown in Figure 2-4. (b) as irregular high energy (green and red) in shading image. The rectangular region in image domain, reflects a significant change before and after BCP procedure in image.

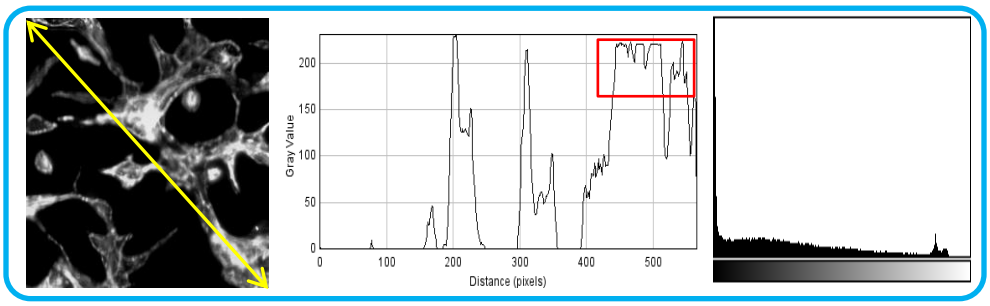

(a) Original set

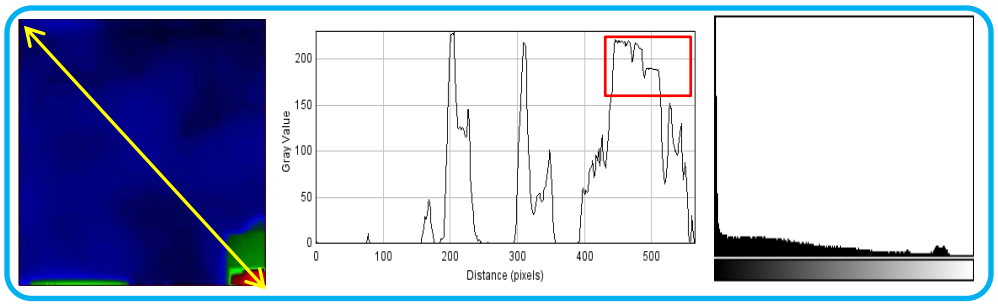

(b) RBA processing

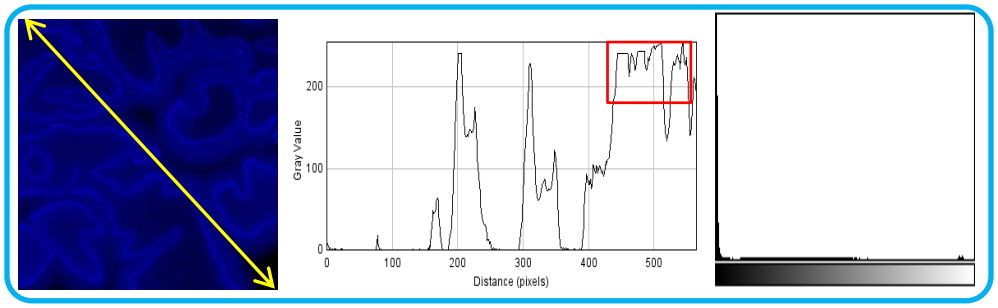

(c) DCBC processing

Figure 2-4. Artefacts removal of cardiomyocytes cell image cultures. (a) Original image, diagonal (along the yellow line) profiling plot and global pixel histogram. (b) and (c) are the strategies of background correction with the resulting shading, diagonal profiling plot and global pixel histogram, RBA and DCBC respectively.

2) Multilevel background subtraction effect:

A well performed BCP procedure would eliminate background signal that present in the image, while preserving the valuable (foreground) signal. Figure 2-5 illustrates the performance of three methods on image sets of cartilage cell cultures (2 weeks, 4 weeks and 7 weeks respectively). The original and the corrected image samples are in the first column, the corresponding surface diagrams (15% Gaussian smoothing processing) are shown in second column, while image global intensity profiles are depicted in the third column. Note that the specified surface plot in Figure 2-5 describes the ability of remaining all information in original foreground and the smoothed and evenly distributed background.

The partitioning of differences in background illumination and foreground is quite difficult in most of the fluorescence and bright-field microscopy images. However in the proposed DCBC method, the information is retained better on the basis of bimodal thresholding strategy, while the distribution of the global intensity is more coherent.

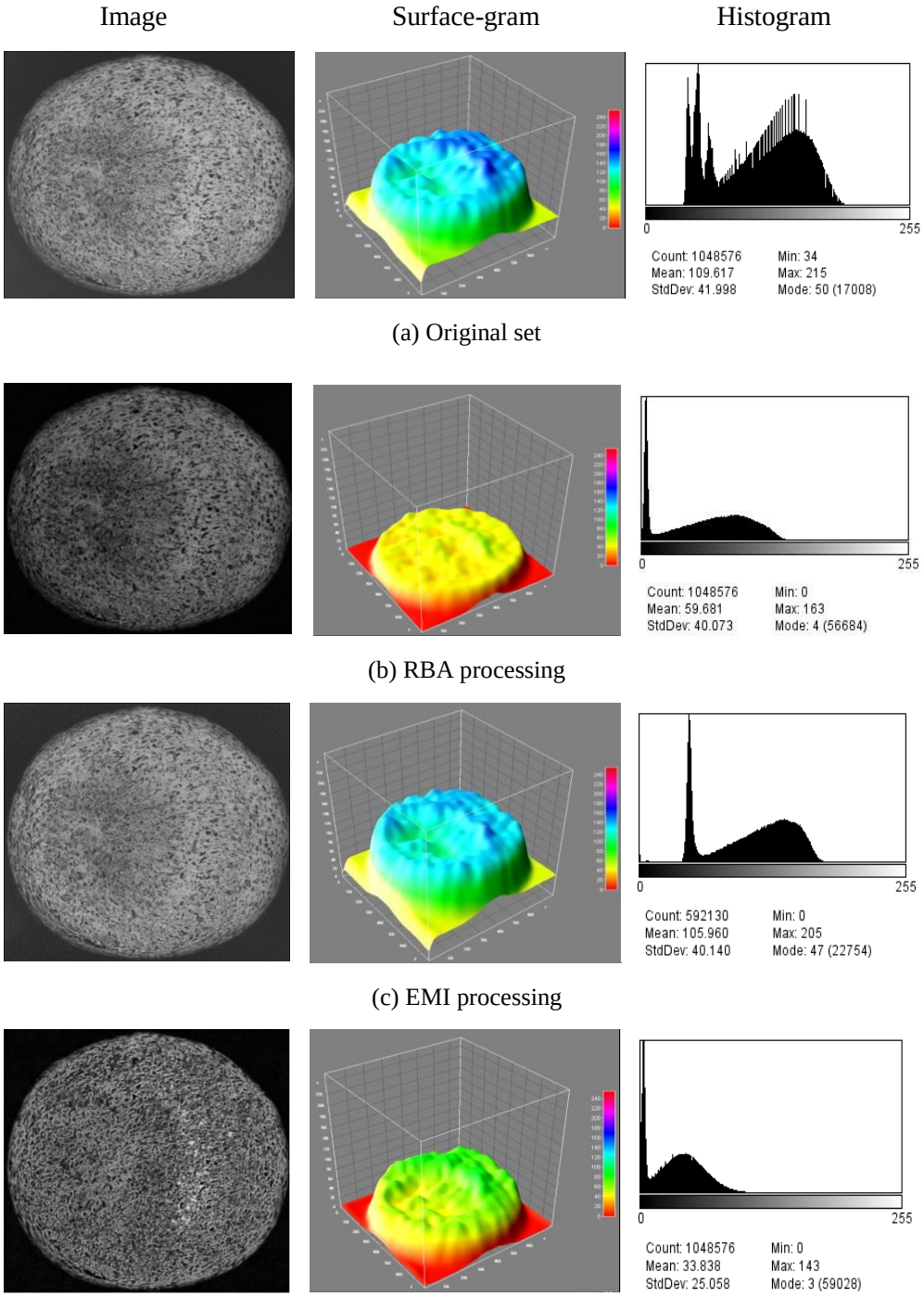

Figure 2-5. Qualitative comparison of different background correction methods in terms of distribution of grey histogram.

C. Quantitative evaluation

To gain insight in proposed method, a widely acceptable index referred to as Coefficient of Joint Variation (CJV) [13] is utilized. The CJV is characterized by invariance to uniform transformation, i.e., multiplicative and additive illumination. This can be extended to a bimodal formulation:

$$CJV(I_1, I_2) = [\mu(I_1) - \mu(I_2)]^{-1}[\sigma(I_1) + \sigma(I_2)] \qquad \textbf{Equation 2-15}$$

Where, CJV is the sum of the standard deviations of images before I_1 and after I_2 BCP procedure, normalized by the difference of their means. The performances of background subtraction methods are quantitatively evaluated compared with a baseline value, which is computed by the variation of global intensity in the intact (original) image. This can be derived as a limiting form of Equation 2-15 as: $CJV_{Baseline}(I_1) = [\mu(I_1)]^{-1}[\sigma(I_1)]$, where post-processing image is regarded as shading-free (global intensity is zero in fluorescence image type, or max-bit value in bright-field image type; while standard deviation equal to zero as well).

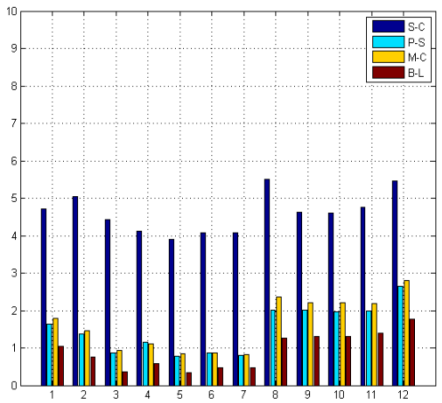

(a) Cartilage weekly #1

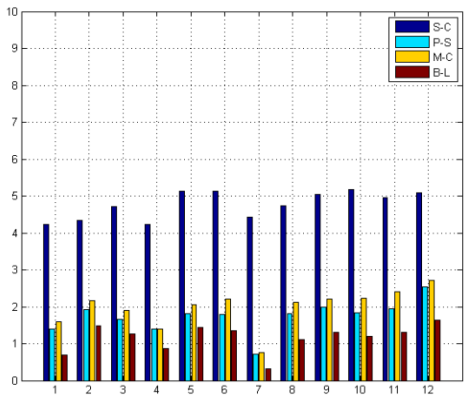

(b) Cartilage weekly #2

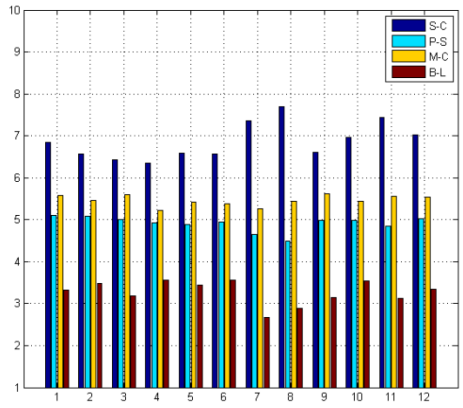

(c) Cardiomyocyte

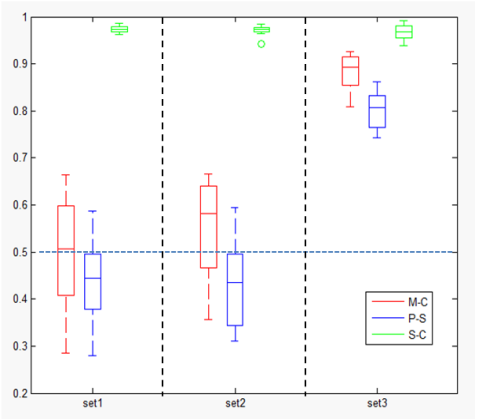

(d) Distribution of changes for CJV

Figure 2-6. Performance of three methodologies compared with baseline on three different datasets (a), (b) and (c) respectively. The CJV values are accordingly evaluated and visualized in (d)

The results of background correction are illustrated in Figure 2-6, in which each subfigure stands for one data set. Three representative under-evaluated methodologies, i.e. entropy minimization for shading correction (S-C), morphological correction in RBA (M-C) and proposed DCBC approach (P-S) are compared with baseline value (B-L). In a case of light microscope images after BCP procedure, an ideal distribution of image variation should have smaller global intensity to guarantee background signals are well-eliminated; while global deviation should stand, at least not larger than the intact image to make sure that there is not any tedious signal is introduced. This means that the methodology obtaining the smallest CJV value that outperforms the others. Given by box-whiskers diagram in Figure 2-6 (d), the statistical variation of CJV is then investigated.

From all independent runs, we obtain the average performance of 12 samples for each datasets in terms of CJV value and shown in Table 2-1. The computing time is then illustrated in Table 2-2 for systematically comparison. The best performances (except baseline index) are marked as bold italic in each table.

Table 2-1. Performance of background correction strategies of three dataset in CJV index

	Set1		Set 2		Set 3	
	ΔStd	Δmean	ΔStd	Δmean	ΔStd	Δmean
RBA (M-C)	0.4489	0.6431	0.3391	0.8029	2.9065	23.688
EMI (S-C)	6.5609	11.4812	4.2305	12.4983	51.1308	105.7754
DCBC(P-S)	**0.3547**	**0.5428**	**0.2541**	**0.6144**	**2.1814**	**13.7637**
Baseline (B-L)	0.1390	0.2808	0.1058	0.3388	0.6952	2.7300

Table 2-2. Time complexity in average (seconds)

	Set 1	Set 2	Set 3
EMI (S-C)	58.67	167.23	458.73
RBA (M-C)	1.84	**2.54**	**4.01**
DCBC(P-S)	**1.59**	3.22	6.15

2.6. Discussion and Conclusion

The impacts of the qualitative comparison of BCP procedure performance are shown in Figure 2-4 and Figure 2-5. These results suggest the following evaluation: (i) In Figure 2-4. (c), compared with (b), shows a much better result in terms of the elimination of artefacts signal (removal of square-like high energy region). (ii) In both the red rectangle region in diagonal intensity plot and shown in global pixel histogram, the proposed method kept most information and the intensities across region (slope in the 2D line change) are enhanced for further analysis. (iii) In Figure 2-5, resulting images of visualisation of cartilage cells are shown, where EMI processing eliminates less background than other methods do. (iv) Image after DCBC processing is shading-free, while has clearer and smoother foreground shape that contains all relevant signal. The dam- constraint strategy prevents the over elimination of mixed illumination, and then a more unambiguous and complete cartilage contour can be seen by visual inspection.

The statistics of the three tested approaches can be investigated via Figure 2-6, Table 2-1 and Table 2-2: (i) Evident differences of CJV expression are observed from Figure 2-6 (a) to (c); the likely ranges and interquartile ranges of variation indicated in figure 6 (d) suggests a better performance of proposed method on the three

datasets. (ii) All methods are accomplished in successfully reducing background, while DCBC method always produces better results in terms of smallest CJV value; specifically in set 1 and set 2, a significant improvement can be noticed with a value change of CJV of more than 50%. (iv) Compared with the baseline in Table 2-1, it can be observed that BCP procedure is essential and efficient by removal of noise and redundancy. (v) Proposed method always has a lower CJV value on various datasets, while has a lower time complexity in set 1. (vi) On the basic definition of prevalent EMI method, a retrospectively procedure for estimating shading components consumes a large time budget in application; while convergent parametric components play a role in equalizing original image, meaning a lesser variation compared with intact image and mostly unchanged global intensity. This results in an insufficient elimination of background in fluorescence and bright-field images, and yielding relatively larger CJV value. (vii) In the proposed method, a dam is erected to constrain a path by utilizing both the fuzzy and rough set framework. The membership function of fuzzy logic can handle overlapping partitions; whereas the lower and upper approximations of rough sets can characterize the vagueness and incompleteness in its bimodal class definition. This results in smoothing of the foreground information and a global minimization of the image intensity, while there is not tedious variation introduced.

In this chapter, we propose a Dam-Constraint Background Correction (DCBC) algorithm, which is a novel hybridized approach. The algorithm successfully overcomes the drawback of existing method and includes fully automated data driven parameter tuning. With the innovated morphological concept in image domain, namely “dam-constraint”, the proposed method outperforms the widely and commonly utilized RBA algorithm and the EMI method in both qualitative and quantitative tests. The new method is very promising for application to microscopy images in which further analysis is hampered by undesired effects to background illumination. The subsequent processing steps in proposed data analysis track will be further illustrated in next chapters.

2.7. References

[1]J. C. Waters, “Accuracy and precision in quantitative fluorescence microscopy.” J. Cell Biol., vol. 185, no. 7, pp. 1135–48, Jun. 2009.

[2]B. Likar, J. B. Maintz, M. a Viergever, and F. Pernus, “Retrospective shading correction based on entropy minimization.” J. Microsc., vol. 197, no. Pt 3, pp. 285–95, Mar. 2000.

[3]M. L. Schultz, L. E. Lipkin, M. J. Wade, P. F. Lemkin, and G. M. Carman, “High Resolution Shading Correction” J. Histochem. Cytochem., vol. 22, no. 7, pp. 751–754, Jul. 1974.

[4]A. J. Hanson, “The Rolling Ball” Graphics Gems III, D.Kirk ed., Academic Press, 1992, pp. 51–60.

[5]P. Hall, B. U. Park, and B. A. Turlach, “Rolling-ball method for estimating the boundary of the support of a point-process intensity” no. June, 1998.

[6]F. Zanella, J. B. Lorens, and W. Link, “High content screening: Seeing is believing” Trends in Biotechnology, vol. 28. pp. 237–245, 2010.

[7]U. S. Navy, “Fuzzy Sets *,” vol. 8, no. 3, pp. 338–353, 1965.

[8]Z. Pawlak, “Rough set approach to knowledge-based decision support” Eur. J. Oper. Res., vol. 99, no. 1, pp. 48–57, May 1997.

[9]M. M. Mushrif and A. K. Ray, “Color image segmentation: Rough-set theoretic approach” Pattern Recognition. Lett., vol. 29, no. 4, pp. 483–493, Mar. 2008.

[10]J. C. Waters and J. R. Swedlow, “Techniques Interpreting Fluorescence Microscopy Images and Measurements” 2008.

[11]A. Petrosino and G. Salvi, “Rough fuzzy set based scale space transforms and their use in image analysis” Int. J. Approx. Reason., vol. 41, no. 2, pp. 212–228, Feb. 2006.

[12]A. De Luca and S. Termini, “A definition of a nonprobabilistic entropy in the setting of fuzzy sets theory” Inf. Control, vol. 20, no. 4, pp. 301–312, May 1972.

[13]B. Likar, M. Viergever, and F. Pernus, “Retrospective correction of MR intensity inhomogeneity by information minimization” Med. Imaging, IEEE, 2001.

[14]Z. Ji, Q. Sun, Y. Xia, Q. Chen, D. Xia, and D. Feng, “Generalized rough fuzzy c-means algorithm for brain MR image segmentation.” Comput. Methods Programs Biomed., vol. 108, no. 2, pp. 644–55, Nov. 2012.

[15] Piccinini, F., Lucarelli, E., Gherardi, A. and Bevilacqua, A., 2012. Multi‐image based method to correct vignetting effect in light microscopy images. Journal of microscopy, 248(1), pp.6-22.

[16] Zwier, J.M., Van Rooij, G.J., Hofstraat, J.W. and Brakenhoff, G.J., 2004. Image calibration in fluorescence microscopy. Journal of Microscopy, 216(1), pp.15-24.

[17] Singh, S., BRAY, M.A., Jones, T.R. and Carpenter, A.E., 2014. Pipeline for illumination correction of images for high‐throughput microscopy. Journal of microscopy, 256(3), pp.231-236.

[18] Leong, F.W., Brady, M. and McGee, J.O.D., 2003. Correction of uneven illumination (vignetting) in digital microscopy images. Journal of clinical pathology, 56(8), pp.619-621.

[19] Poon, S.S., Wong, J.T., Saunders, D.N., Ma, Q.C., McKinney, S., Fee, J. and Aparicio, S.A., 2008. Intensity calibration and automated cell cycle gating for high‐throughput image‐based siRNA screens of mammalian cells. Cytometry Part A, 73(10), pp.904-917.

[20] LEE, S.C. and Bajcsy, P., 2006. Intensity correction of fluorescent confocal laser scanning microscope images by mean‐weight filtering. Journal of microscopy, 221(2), pp.122-136.

[21] Huang, Adam, Chung-Wei Lee, and Hon-Man Liu. "Rolling ball sifting algorithm for the augmented visual inspection of carotid bruit auscultation." Scientific Reports 6 (2016).